Article

Metal Ion-Promoted Intramolecular Electron Transfer in a Ferrocene-Naphthoquinone Linked Dyad. Continuous Change in Driving Force and Reorganization Energy with Metal Ion Concentration

Ken Okamoto, Hiroshi Imahori, and Shunichi Fukuzumi

J. Am. Chem. Soc., **2003**, 125 (23), 7014-7021• DOI: 10.1021/ja034831r • Publication Date (Web): 15 May 2003

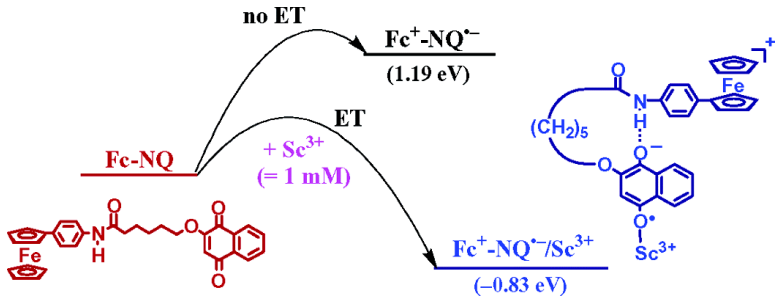

More About This Article

Additional resources and features associated with this article are available within the HTML version:

- Supporting Information
- Links to the 6 articles that cite this article, as of the time of this article download
- Access to high resolution figures
- Links to articles and content related to this article
- Copyright permission to reproduce figures and/or text from this article

View the Full Text HTML

J|A|C|S
ARTICLES
Published on Web 05/15/2003

Metal Ion-Promoted Intramolecular Electron Transfer in a Ferrocene-Naphthoquinone Linked Dyad. Continuous Change in Driving Force and Reorganization Energy with Metal Ion Concentration

Ken Okamoto,[†] Hiroshi Imahori,*[,‡] and Shunichi Fukuzumi*[,†]

Contribution from the Department of Material and Life Science, Graduate School of Engineering, Osaka University, CREST, Japan Science and Technology Corporation, Suita, Osaka 565-0871, Japan, Department of Molecular Engineering, Graduate School of Engineering, Kyoto University, PRESTO, Japan Science and Technology Corporation (JST), Sakyo-ku, Kyoto 606-8501, Japan, and Fukui Institute for Fundamental Chemistry, Kyoto University, 34-4, Takano-Nishihiraki-cho, Sakyo-ku, Kyoto 606-8103, Japan

Received February 24, 2003; E-mail: fukuzumi@ap.chem.eng.osaka-u.ac.jp; imahori@sci.kyoto-u.ac.jp

Abstract: Thermal intramolecular electron transfer from the ferrocene (Fc) to naphthoquinone (NQ) moiety occurs efficiently by the addition of metal triflates (M^{n+}: $Sc(OTf)_3$, $Y(OTf)_3$, $Eu(OTf)_3$) to an acetonitrile solution of a ferrocene-naphthoquinone (**Fc-NQ**) linked dyad with a flexible methylene and an amide spacer, although no electron transfer takes place in the absence of M^{n+}. The resulting semiquinone radical anion ($NQ^{\bullet-}$) is stabilized by the strong binding of M^{n+} with one carbonyl oxygen of $NQ^{\bullet-}$ as well as hydrogen bonding between the amide proton and the other carbonyl oxygen of $NQ^{\bullet-}$. The high stability of the $\mathbf{Fc^{+}\text{-}NQ^{\bullet-}/M^{n+}}$ complex allows us to determine the driving force of electron transfer by the conventional electrochemical method. The one-electron reduction potential of the NQ moiety of **Fc-NQ** is shifted to a positive direction with increasing concentration of M^{n+}, obeying the Nernst equation, whereas the one-electron oxidation potential of the Fc moiety remains the same. The driving force dependence of the observed rate constant (k_{ET}) of M^{n+}-promoted intramolecular electron transfer is well evaluated in light of the Marcus theory of electron transfer. The driving force of electron transfer increases with increasing concentration of M^{n+} [M^{n+}], whereas the reorganization energy of electron transfer decreases with increasing [M^{n+}] from a large value which results from the strong binding between $NQ^{\bullet-}$ and M^{n+}.

Introduction

Electron transfer plays a pivotal role not only in chemical processes but also in biological redox processes that have tremendous relevance to our life such as photosynthesis and respiration.[1−4] To understand factors to control important electron-transfer processes in biological systems, electron-transfer dynamics between donor and acceptor molecules bound to proteins have been studied extensively.[5,6] A number of donor−acceptor linked systems with inert rigid spacers have also been developed to study the intramolecular electron-transfer reactions between the donor (D) and acceptor (A) molecules at a fixed distance.[7−15] The electron-transfer dynamics between D and A at a fixed distance are now well understood in light of

[†] Osaka University.
[‡] Kyoto University.

(1) *Electron Transfer in Chemistry*; Balzani, V., Ed.; Wiley-VCH: Weinheim, 2001; Vols. 1−5.
(2) (a) *Anoxygenic Photosynthetic Bacteria*; Blankenship, R. E., Madigan, M. T., Bauer, C. E., Eds.; Kluwer Academic Publishing: Dordrecht, 1995. (b) Armstrong, F. A.; Kaim, W.; Schwederski, B. *Bioinorganic Chemistry: Inorganic Chemistry in the Chemistry of Life*; Oxford University: U.K., 1995.
(3) (a) Kochi, J. K. *Acc. Chem. Res.* **1992**, *25*, 39. (b) Rathore, R.; Kochi, J. K. *Adv. Phys. Org. Chem.* **2000**, *35*, 193.
(4) (a) Fukuzumi, S. In *Advances in Electron-Transfer Chemistry*; Mariano, P. S., Ed.; JAI Press: Greenwich, CT, 1992; pp 67−175. (b) Fukuzumi, S.; Tanaka, T. In *Photoinduced Electron Transfer*; Fox, M. A., Chanon, M., Eds.; Elsevier: Amsterdam, 1988; Part C, Chapter 10.
(5) (a) Winkler, J. R.; Gray, H. B. *Chem. Rev.* **1992**, *92*, 369. (b) McLendon, G.; Hake, R. *Chem. Rev.* **1992**, *92*, 481. (c) Isied, S. S.; Ogawa, M. Y.; Wishart, J. F. *Chem. Rev.* **1992**, *92*, 381. (d) Tollin, G. In *Electron Transfer in Chemistry*; Balzani, V., Ed.; Wiley-VCH: Weinheim, 2001; Vol. 4, pp 202−231.
(6) (a) Moser, C. C.; Keske, J. M.; Warncke, K.; Farid, R. S.; Dutton, P. L. *Nature* **1992**, *355*, 796. (b) Kirmaier, C.; Holton, D. In *The Photosynthetic Reaction Center*; Deisenhofer, J., Norris, J. R., Eds.; Academic Press: San Diego, 1993; Vol. II, pp 49−70. (c) Langen, R.; Chang, I.-J.; Germanas, J. P.; Richards, J. H.; Winkler, J. R.; Gray, H. B. *Science* **1995**, *268*, 1733. (d) Page, C. C.; Moser, C. C.; Chen, X.; Dutton, P. L. *Nature* **1999**, *402*, 47.
(7) (a) Gust, D.; Moore, T. A. In *The Porphyrin Handbook*; Kadish, K. M., Smith, K. M., Guilard, R., Eds.; Academic Press: San Diego, CA, 2000; Vol. 8, pp 153−190. (b) Gust, D.; Moore, T. A.; Moore, A. L. In *Electron Transfer in Chemistry*; Balzani, V., Ed.; Wiley-VCH: Weinheim, 2001; Vol. 3, pp 272−336. (c) Kurreck, H.; Huber, M. *Angew. Chem., Int. Ed. Engl.* **1995**, *34*, 849. (d) Gust, D.; Moore, T. A.; Moore, A. L. *Acc. Chem. Res.* **2001**, *34*, 40.
(8) (a) Imahori, H.; Sakata, Y. *Adv. Mater.* **1997**, *9*, 537. (b) Imahori, H.; Sakata, Y. *Eur. J. Org. Chem.* **1999**, *2445*, 5. (c) Fukuzumi, S.; Imahori, H. In *Electron Transfer in Chemistry*; Balzani, V., Ed.; Wiley-VCH: Weinheim, 2001; Vol. 2, pp 927−975.
(9) (a) Wasielewski, M. R. In *Photoinduced Electron Transfer*; Fox, M. A., Chanon, M., Eds.; Elsevier: Amsterdam, 1988; Part A, pp 161−206. (b) Wasielewski, M. R. *Chem. Rev.* **1992**, *92*, 435.
(10) (a) Paddon-Row, M. N. In *Electron Transfer in Chemistry*; Balzani, V., Ed.; Wiley-VCH: Weinheim, 2001; Vol. 3, pp 179−271. (b) Jordan, K. D.; Paddon-Row, M. N. *Chem. Rev.* **1992**, *92*, 395. (c) Paddon-Row, M. N. *Acc. Chem. Res.* **1994**, *27*, 18.
(11) Verhoeven, J. W. *Adv. Chem. Phys.* **1999**, *106*, 603.

10.1021/ja034831r CCC: $25.00

the Marcus theory of electron transfer.[16] Once the driving force ($-\Delta G_{ET}^0$) and reorganization energy (λ_{DA}) of electron transfer between D and A are determined, the activation free energy of electron transfer ($\Delta G^{\ddagger}_{ET}$) is well predicted using the Marcus equation (eq 1).[16]

$$\Delta G^{\ddagger}_{ET} = (\lambda_{DA}/4)(1 + \Delta G_{ET}^0/\lambda_{DA})^2 \quad (1)$$

The driving force of electron transfer is obtained from the one-electron oxidation potential of electron donor (E_{ox}^0) and the one-electron reduction potential of electron acceptor (E_{red}^0) using eq 2, where F is the Faraday constant. The reorganization energy

$$\Delta G_{ET}^0 = F(E_{ox}^0 - E_{red}^0) \quad (2)$$

of electron transfer between D and A (λ_{DA}) is obtained as the average of the reorganization energy for the electron self-exchange between D and $D^{\bullet+}$ (λ_D) and that between A and $A^{\bullet-}$ (λ_A): eq 3.[16] Thus, knowledge of the fundamental redox properties of D (E_{ox}^0 and λ_D) and A (E_{red}^0 and λ_A) is sufficient

$$\lambda_{DA} = (\lambda_D + \lambda_A)/2 \quad (3)$$

to predict the $\Delta G^{\ddagger}_{ET}$ values using eq 1.[16,17] In other words, the electron-transfer reactivity is automatically determined once the combination of D and A is fixed. However, it has recently been demonstrated that the scope of electron-transfer reactivity can be expanded much further by introducing a third component such as a metal ion to the D−A system provided that the metal ion can interact with one of the products of electron transfer, for example, the radical anion ($A^{\bullet-}$).[18,19] Although photoexcitation of the D or A moiety or radiolysis is normally required to start the electron transfer of the D−A linked system, thermal intramolecular electron-transfer reactions of D−A linked systems, which would otherwise never occur, can be started by the addition of the appropriate metal ions.[20,21] There have also been a number of examples of metal ion-promoted intermolecular electron-transfer reactions.[22−26] In biological redox systems, a variety of metal ion enzymes are also involved to finely control electron-transfer processes.[1] In the case of metal ion-promoted electron-transfer reactions between D and A, the driving force of electron transfer is altered by the addition of metal ions which can interact with $A^{\bullet-}$. However, the instability of the metal ion complexes with $A^{\bullet-}$ has precluded the determination of the one-electron reduction potentials of A in the presence of metal ions. As such, the driving force dependence of rates of metal ion-promoted electron-transfer reactions has yet to be examined. Moreover, the reorganization energy of electron transfer is also expected to be altered in the presence of metal ions, because the binding of metal ions associated with electron transfer certainly requires a much larger reorganization energy than the value without metal ion. Under such circumstances, the applicability of the Marcus equation (eq 1) to metal ion-promoted electron-transfer reactions has remained unexplored as compared to well-established electron-transfer processes involving only D and A.

Scheme 1

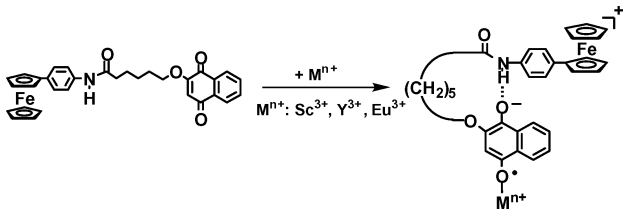

We report herein the driving force dependence of metal ion-promoted intramolecular electron transfer. The results are evaluated in light of the Marcus theory of electron transfer. The D−A system employed in this study is a ferrocene-naphthoquinone dyad (**Fc-NQ**) in which the metal ion-promoted thermal intramolecular electron-transfer reaction proceeds efficiently (Scheme 1). The metal ion complexes with $NQ^{\bullet-}$ moiety of **Fc-NQ** are stable enough to determine the one-electron reduction potentials of **Fc-NQ** in the presence of metal ion. This enables us to determine the driving force of metal ion-promoted electron transfer and hence to examine the driving force dependence of the electron-transfer dynamics in light of the Marcus theory of electron transfer.

Experimental Section

General. ^{1}H NMR spectra were measured on a JEOL JNM-AL300 NMR spectrometer. Fast atom bombardment mass spectra (FAB-MS) were obtained on a JEOL JMS-DX300 mass spectrometer. Melting points were recorded on a Yanagimoto micro-melting point apparatus and not corrected. IR spectra were measured on a Shimadzu FT-IR 8200 PC as KBr disks. Elemental analyses were performed on a Perkin-Elmer model 240C elemental analyzer.

Materials. All solvents and chemicals were of reagent grade quality, obtained commercially, and used without further purification unless otherwise noted. Tris(2,2′-bipyridyl)ruthenium(III) hexafluorophosphate [$Ru(bpy)_3(PF_6)_3$] was prepared according to the literature.[27] Scandium triflate [$Sc(OTf)_3$ (99%, FW = 492.16)] was purchased from Pacific

(12) (a) Chambron, J. C.; Chardon-Noblat, S.; Harriman, A.; Heitz, V.; Sauvage, J.-P. *Pure Appl. Chem.* **1993**, *65*, 2343. (b) Harriman, A.; Sauvage, J.-P. *Chem. Soc. Rev.* **1996**, *25*, 41. (c) Blanco, M.-J.; Consuelo Jiménez, M.; Chambron, J.-C.; Heitz, V.; Linke, M.; Sauvage, J.-P. *Chem. Soc. Rev.* **1999**, *28*, 293.
(13) (a) Balzani, V.; Juris, A.; Venturi, M.; Campagna, S.; Serroni, S. *Chem. Rev.* **1996**, *96*, 759. (b) Scandola, F.; Chiorboli, C.; Indelli, M. T.; Rampi, M. A. In *Electron Transfer in Chemistry*; Balzani, V., Ed.; Wiley-VCH: Weinheim, 2001; Vol. 3, pp 337−408.
(14) (a) Maruyama, K.; Osuka, A.; Mataga, N. *Pure Appl. Chem.* **1994**, *66*, 867. (b) Osuka, A.; Mataga, N.; Okada, T. *Pure Appl. Chem.* **1997**, *69*, 797. (c) Piotrowiak, P. *Chem. Soc. Rev.* **1999**, *28*, 143.
(15) (a) Guldi, D. M. *Chem. Commun.* **2000**, 321. (b) Guldi, D. M.; Prato, M. *Acc. Chem. Res.* **2000**, *33*, 695.
(16) (a) Marcus, R. A. *Annu. Rev. Phys. Chem.* **1964**, *15*, 155. (b) Marcus, R. A. *Angew. Chem., Int. Ed. Engl.* **1993**, *32*, 1111. (c) Marcus, R. A.; Sutin, N. *Biochim. Biophys. Acta* **1985**, *811*, 265.
(17) (a) Eberson, L. *Adv. Phys. Org. Chem.* **1982**, *18*, 79. (b) Eberson, L. *Electron-Transfer Reactions in Organic Chemistry; Reactivity and Structure*; Springler: Heidelberg, 1987; Vol. 25.
(18) Fukuzumi, S. In *Electron Transfer in Chemistry*; Balzani, V., Ed.; Wiley-VCH: Weinheim, 2001; Vol. 4, pp 3−67.
(19) (a) Fukuzumi, S. *Org. Biomol.* **2003**, *1*, 609. (b) Fukuzumi, S.; Itoh, S. In *Advances in Photochemistry*; Neckers, D. C., Volman, D. H., von Bünau, G., Eds.; Wiley: New York, 1998; Vol. 25, pp 107−172.
(20) Fukuzumi, S.; Okamoto, K.; Imahori, H. *Angew. Chem., Int. Ed.* **2002**, *41*, 620.
(21) Fukuzumi, S.; Okamoto, K.; Yoshida, Y.; Imahori, H.; Araki, Y.; Ito, O. *J. Am. Chem. Soc.* **2003**, *125*, 1007.
(22) (a) Fukuzumi, S.; Koumitsu, S.; Hironaka, K.; Tanaka, T. *J. Am. Chem. Soc.* **1987**, *109*, 305. (b) Fukuzumi, S.; Nishizawa, N.; Tanaka, T. *J. Chem. Soc., Perkin Trans. 2* **1985**, 371.
(23) Fukuzumi, S.; Ohkubo, K. *Chem.-Eur. J.* **2000**, *6*, 4532.
(24) (a) Fukuzumi, S.; Okamoto, T.; Otera, J. *J. Am. Chem. Soc.* **1994**, *116*, 5503. (b) Fukuzumi, S.; Satoh, N.; Okamoto, T.; Yasui, K.; Suenobu, T.; Seko, Y.; Fujitsuka, M.; Ito, O. *J. Am. Chem. Soc.* **2001**, *123*, 7756.
(25) (a) Fukuzumi, S.; Mori, H.; Imahori, H.; Suenobu, T.; Araki, Y.; Ito, O.; Kadish, K. M. *J. Am. Chem. Soc.* **2001**, *123*, 12458. (b) Fukuzumi, S.; Fujii, Y.; Suenobu, T. *J. Am. Chem. Soc.* **2001**, *123*, 10191.
(26) (a) Fukuzumi, S.; Ohkubo, K.; Okamoto, T. *J. Am. Chem. Soc.* **2002**, *124*, 14147. (b) Fukuzumi, S.; Inada, O.; Satoh, N.; Suenobu, T.; Imahori, H. *J. Am. Chem. Soc.* **2002**, *124*, 9181. (c) Fukuzumi, S.; Yuasa, J.; Suenobu, T. *J. Am. Chem. Soc.* **2002**, *124*, 12566.
(27) DeSimone, R. E.; Drago, R. S. *J. Am. Chem. Soc.* **1970**, *92*, 2343.

Scheme 2

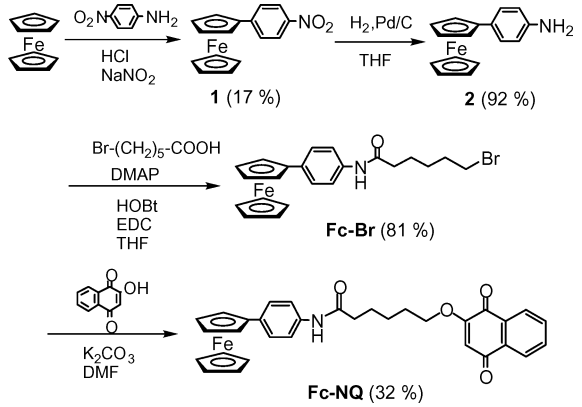

Metals Co., Ltd. (Taiheiyo Kinzoku). Yttrium triflate [$Y(OTf)_3$] and europium triflate [$Eu(OTf)_3$] were prepared by the literature method.[28] Metal triflates were dried under vacuum evacuation at 403 K for 40 h prior to use. Magnesium perchlorate [$Mg(ClO_4)_2$] and barium perchlorate [$Ba(ClO_4)_2$] were obtained from Wako Pure Chemical Ind. Ltd., Japan. Acetonitrile (MeCN) used as a solvent was purified and dried by the standard procedure.[29] Chloroform-*d* was obtained from EURI SO-TOP, CEA, France. Thin-layer chromatography (TLC) and flash column chromatography were performed with Art. 5554 DC-Alufolien Kieselgel 60 F_{254} (Merck), and Fujisilica BW300, respectively.

Synthesis. The synthetic route to **Fc-NQ** is summarized in Scheme 2. Ferrocene derivatives **1** and **2** were prepared according to the literature.[30]

Fc-Br. A solution of THF containing 4-(dimethylamino)pyridine (DMAP: 200 mg, 1.06 mmol), 1-hydroxybenzotriazole (HOBt: 160 mg, 1.19 mmol), and 6-bromohexanoic acid (800 mg, 4.10 mmol) was treated with 1-ethyl-3-(3-dimethylaminopropyl)carbodiimide hydrochloride (EDC: 400 mg, 2.08 mmol) under nitrogen at 0 °C. The mixture was stirred for 1 h at 0 °C. 4-Aminophenylferrocene (**2**) (150 mg, 0.54 mmol) was added to the mixture and stirred at 0 °C for 30 min. The mixture was then stirred at room temperature overnight. The mixture was concentrated in vacuo and poured into a 5% HCl aqueous solution and extracted with chloroform (50 mL × 3). The crude product was purified by flash chromatography (SiO_2, EtOAc:$CHCl_3$ = 1:10, R_f = 0.67). Subsequent recrystallization from chloroform and hexane gave **Fc-Br** as an orange solid (200 mg, 0.44 mmol, 81%). ^{1}H NMR (300 MHz, $CDCl_3$): δ 7.43 (s, 4H), 7.08 (s, 1H), 4.60 (t, 2H, J = 2 Hz), 4.29 (t, 2H, J = 2 Hz), 4.03 (s, 5H), 3.43 (t, 2H, J = 7 Hz), 2.39 (t, 2H, J = 7 Hz), 1.92 (q, 2H, J = 7 Hz), 1.79 (q, 2H, J = 7 Hz), 1.64 (q, 2H, J = 7 Hz). ^{13}C NMR (300 MHz, $CDCl_3$): δ 159.5 (amide, C═O), 136.1 (Ph), 126.6 (Fc), 119.8 (Ph), 37.5 (O═C−CH_2−), 33.7 (−CH_2−Br), 32.4 (−CH_2−), 27.8 (−CH_2−), 24.8 (−CH_2−). FAB-MS *m*/*z* 455, 453. Anal. Calcd for $C_{22}H_{24}BrFeNO$: C, 58.18; H, 5.33; N, 3.08; Br, 17.59. Found: C, 58.10; H, 5.21; N, 3.17; Br, 17.47. FT-IR (KBr): 1700, 1650, 1620, 1580 cm^{-1}. mp 135.5−137.5 °C.

Fc-NQ. A solution of DMF containing 2-hydroxy-1,4-naphthoquinone (900 mg, 5.17 mmol), **Fc-Br** (150 mg, 0.33 mmol), and dehydrated potassium carbonate (600 mg, 4.35 mmol) was stirred under nitrogen at room temperature for 10 min. The reaction mixture was then refluxed for 30 min. The mixture was evacuated in vacuo. The crude product was purified by flash chromatography (SiO_2, EtOAc:$CHCl_3$ = 1:10, R_f = 0.27). The brown fraction was concentrated in vacuo. Subsequent recrystallization from chloroform and hexane gave **Fc-NQ** as a brown solid (55 mg, 0.10 mmol, 32%). ^{1}H NMR (300 MHz, $CDCl_3$): δ 8.11 (ddd, 2H, J = 2, 2, 7 Hz), 7.74 (ddd, 2H, J = 2, 7, 7 Hz), 7.45 (m, 4H), 7.42 (s, 1H), 6.16 (s, 1H), 4.60 (t, 2H, J = 2 Hz), 4.29 (t, 2H, J = 2 Hz), 4.06 (t, 2H, J = 7 Hz), 4.03 (s, 5H), 2.44 (t, 2H, J = 7 Hz), 1.97 (q, 2H, J = 7 Hz), 1.90 (q, 2H, J = 7 Hz), 1.64 (q, 2H, J = 7 Hz). ^{13}C NMR (300 MHz, $CDCl_3$): δ 184.9 (NQ, C═O), 171.1 (NQ, C═O), 159.7 (amide, C═O), 136.0 (Ph), 135.2 (NQ), 134.4 (NQ), 133.3 (NQ), 132.1 (NQ), 131.3 (NQ), 126.7 (Fc), 126.5 (Fc), 126.2 (Fc), 119.8 (Ph), 110.3 (NQ), 66.2 (−CH_2−O), 37.5 (O═C−CH_2), 27.6 (−CH_2−), 26.0 (−CH_2−), 25.2 (−CH_2−). FAB-MS *m*/*z* 547. Anal. Calcd for $C_{32}H_{29}FeNO_4$: C, 70.21; H, 5.34; N, 2.56. Found: C, 69.81; H, 5.41; N, 2.44. FT-IR (KBr): 1700, 1680, 1650, 1610, 1580 cm^{-1}. mp 130.0−132.0 °C.

Spectral Measurements. The formation of the $\mathbf{Fc^+}$-$\mathbf{NQ^{\bullet -}}$/$\mathbf{Sc^{3+}}$ complex was examined from the change in the UV−visible spectrum of an MeCN solution of Fc-NQ in the presence of M^{n+} by using a Hewlett-Packard 8453 diode array spectrophotometer with a quartz cuvette (path length = 10 mm) at 298 K.

Kinetic Measurements. Kinetics measurements of intramolecular ET reactions from the ferrocene moiety to naphthoquinone moiety in donor−acceptor systems in the presence of M^{n+} were performed on a Hewlett-Packard 8453 diode array spectrophotometer when the rates were slow enough to be determined accurately. When the rates were too fast (<10 s) to be followed by the photodiode array spectrophotometer, kinetics measurements were performed on a UNISOKU RSP-601 stopped-flow spectrophotometer with the MOS-type high selective photodiode array at various temperature (243−298 K) using a Unisoku thermostated cell holder designed for low-temperature experiments.

Electrochemical Measurements. Electrochemical measurements were performed on a BAS 100 W electrochemical analyzer in deaerated MeCN containing 0.1 M Bu_4NPF_6 ($TBAPF_6$) as supporting electrolyte at 298 K. A conventional three-electrode cell was used with a platinum working electrode (surface area of 0.3 mm^2), and a platinum wire was used as the counter electrode. The Pt working electrode (BAS) was routinely polished with a BAS polishing alumina suspension and rinsed with acetone before use. The measured potentials were recorded with respect to the $Ag/AgNO_3$ (0.01 M) reference electrode. The second-harmonic alternating current voltammetry (SHACV) measurements of Fc-NQ in the presence of $Y(OTf)_3$ were carried out with a BAS 100B electrochemical analyzer in deaerated MeCN containing 0.1 M Bu_4NPF_6 ($TBAPF_6$) as supporting electrolyte.[31] All potentials (vs Ag/Ag^+) were converted to values versus SCE by adding 0.29 V.[32] All electrochemical measurements were carried out under an atmospheric pressure of Ar.

ESR Measurements. The ESR spectra of $\mathbf{Fc\text{-}NQ^{\bullet -}}$ and 2-methoxy-1,4-naphthoquinone radical anion (2-MeO$NQ^{\bullet -}$) were produced by the chemical reduction with the naphthalene radical anion generated by naphthalene (0.5 g) in THF with sodium (0.075 g). The concentration of the naphthalene radical anion was determined by the appearance of the absorption band at the characteristic peak of the semiquinone radical anion (ϵ (422 nm) = 6.0 × 10^3 M^{-1} cm^{-1} in MeCN) produced by the titration of the naphthalene radical anion to *p*-benzoquinone. The solution containing the radical anion was transferred to an ESR tube under an atmospheric pressure of Ar. The ESR spectra were recorded on a JEOL X-band spectrometer (JES-RE1XE) with a quartz ESR tube (1.2 mm i.d.). The ESR spectra were measured under nonsaturating microwave power conditions. The magnitude of modulation was chosen

(28) (a) Forsberg, J. H.; Spaziano, V. T.; Balasubramanian, T. M.; Liu, G. K.; Kinsley, S. A.; Duckworth, C. A.; Poteruca, J. J.; Brown, P. S.; Miller, J. L. *J. Org. Chem.* **1987**, *52*, 1017. (b) Kobayashi, S.; Hachiya, I. *J. Org. Chem.* **1994**, *59*, 3590.
(29) Perrin, D. D.; Armarego, W. L. F.; Perrin, D. R. *Purification of Laboratory Chemicals*, 4th ed.; Pergamon Press: Elmsford, NY, 1996.
(30) Imahori, H.; Tamaki, K.; Guldi, D. M.; Luo, C.; Fujitsuka, M.; Ito, O.; Sakata, Y.; Fukuzumi, S. *J. Am. Chem. Soc.* **2001**, *123*, 2607.
(31) The SHACV method provides a superior approach to directly evaluating the one-electron redox potentials in the presence of a follow-up chemical and reaction, relative to the better-known dc and fundamental harmonic ac methods. See: (a) McCord, T. G.; Smith, D. E. *Anal. Chem.* **1969**, *41*, 1423. (b) Bond, A. M.; Smith, D. E. *Anal. Chem.* **1974**, *46*, 1946. (c) Wasielewski, M. R.; Breslow, R. *J. Am. Chem. Soc.* **1976**, *98*, 4222. (d) Arnett, E. M.; Amarnath, K.; Harvey, N. G.; Cheng, J. *J. Am. Chem. Soc.* **1990**, *112*, 344. (e) Patz, M.; Mayr, H.; Maruta, J.; Fukuzumi, S. *Angew. Chem., Int. Ed. Engl.* **1995**, *34*, 1225.
(32) Mann, C. K.; Barnes, K. K. *Electrochemical Reactions in Nonaqueous Systems*; Marcel Dekker: New York, 1990.

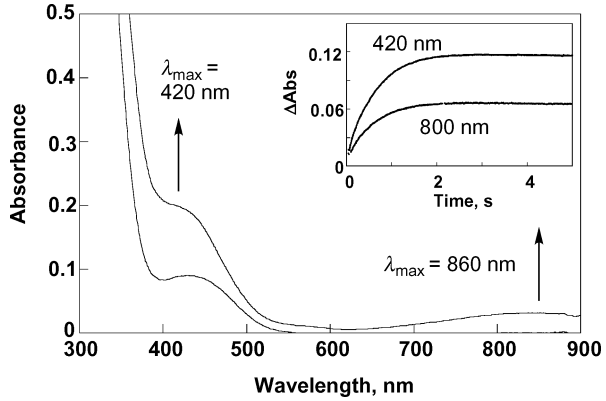

Figure 1. UV−vis spectral change after the addition of Sc^{3+} (1.0×10^{-3} M) into a deaerated MeCN containing **Fc-NQ** (2.0×10^{-4} M) at 298 K. Inset: Time course of the absorption change at 420 and 800 nm due to formation of the $\mathbf{Fc^{+-}NQ^{\bullet-}/Sc^{3+}}$ complex.

to optimize the resolution and the signal-to-noise (*S*/*N*) ratio of the observed spectra. The *g* values were calibrated with an Mn^{2+} marker, and the hyperfine coupling (hfc) constants were determined by computer simulation using the Calleo ESR version 1.2 program coded by Calleo Scientific on an Apple Macintosh personal computer.

Theoretical Calculations. Density functional (DFT) calculations were performed with a basis function: double-ζ Slater-type orbital set (frozen core: C (1s), N (1s), O (1s); ADF basis set II (large)) on a COMPAQ DS20E computer using the Amsterdam density functional (ADF) program version 1999.02 developed by Baerends et al.[33] The gradient corrections of Becke88 (exchange) and Perdew86 (correlation) were included in the exchange-correlation functional. The hfc values are derived from multiplying 506.82 and the spin density values of each hydrogen.

Results and Discussion

Metal Ion-Promoted Intramolecular Electron Transfer. No electron transfer from the ferrocene (Fc) to naphthoquinone (NQ) moiety occurs in **Fc-NQ** with a flexible methylene spacer including an amide linkage thermally in MeCN at 298 K, as expected from the highly positive value of free energy change of electron transfer ($\Delta G_{ET}^0 = 1.19$ eV). However, addition of scandium triflate ($Sc(OTf)_3$: 1.0×10^{-3} M) to an MeCN solution of **Fc-NQ** (2.0×10^{-3} M) results in the formation of Fc^+ as indicated by the appearance of the absorption band due to Fc^+ at 860 nm[34] with the absorption band at $\lambda_{max} = 420$ nm (Scheme 1, Figure 1). This indicates that an intramolecular electron transfer occurs in the presence of Sc^{3+} to produce $\mathbf{Fc^+}$-$\mathbf{NQ^{\bullet-}/Sc^{3+}}$ in which Sc^{3+} is bound to $NQ^{\bullet-}$ and that the absorption band at 420 nm is due to the $NQ^{\bullet-}/Sc^{3+}$ complex. The rates of appearance of the absorption band at 420 and 800 nm obeyed first-order kinetics, and the same first-order rate constants (k_{ET}) were obtained from the first-order plots at 420 and 800 nm. The k_{ET} values determined at 420 nm increase linearly with increasing $[Sc^{3+}]$, $[Y^{3+}]$, and $[Eu^{3+}]$, respectively (Figure 2). The first-order dependence of k_{ET} on $[M^{n+}]$ is consistent with the complexation of one Sc^{3+} with the $NQ^{\bullet-}$ moiety in $\mathbf{Fc^+}$-$\mathbf{NQ^{\bullet-}}$. The binding strength of $NQ^{\bullet-}$ with M^{n+} is expected to vary depending on the Lewis acidity of M^{n+}.[23,35] The replacement of Sc^{3+} by weaker acids such as Y^{3+} and Eu^{3+} results in a slower electron-transfer rate, and by much weaker Lewis acids such as Ba^{2+}, Ca^{2+}, and Mg^{2+} results in no occurrence of electron transfer from Fc to NQ in **Fc-NQ**. The k_{ET} values determined in the presence of various concentrations of M^{n+} are summarized in Table 1.

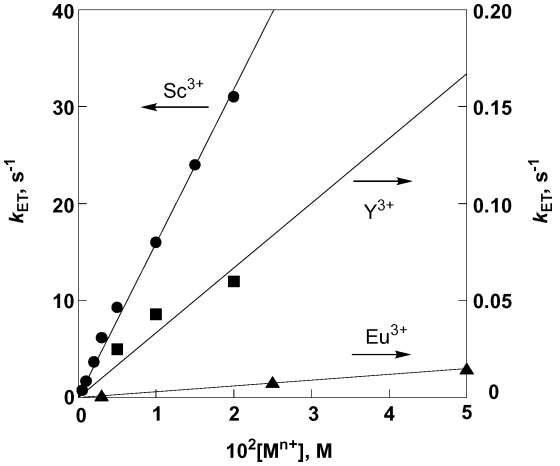

Figure 2. Plots of the rate constant (k_{ET}) determined at 420 nm versus concentration of M^{n+} for M^{n+}-promoted intramolecular ET of **Fc-NQ** (2.0×10^{-4} M) in deaerated MeCN at 298 K.

Table 1. First-Order Rate Constants (k_{ET}), Driving Forces ($-\Delta G_{ET}$), Reorganization Energies (λ), and Activation Free Energies ($\Delta G_{ET}^{\ddagger}$) of Metal Ion-Promoted Intramolecular Electron Transfer in **Fc-NQ** with Various Metal Ion Concentrations $[M^{n+}]$ in Deaerated MeCN at 298 K

M^{n+}	$[M^{n+}]$, M	k_{ET}, s^{-1}	$-\Delta G_{ET}$, eV[a]	λ, eV	$\Delta G_{ET}^{\ddagger}$, eV[b]
Sc^{3+}	5.0×10^{-4}	0.76	0.810	4.53	0.764
	1.0×10^{-3}	1.7	0.828	4.46	0.739
	2.0×10^{-3}	3.7	0.846	4.42	0.722
	3.0×10^{-3}	6.2	0.856	4.38	0.709
	5.0×10^{-3}	9.3	0.869	4.36	0.699
	1.0×10^{-2}	16	0.887	4.33	0.684
	1.0×10^{-2}	24	0.897	4.31	0.676
	2.0×10^{-2}	31	0.905	4.29	0.668
Y^{3+}	5.0×10^{-3}	0.025	0.506	4.36	0.852
	1.0×10^{-2}	0.043	0.523	4.34	0.839
	2.0×10^{-2}	0.060	0.541	4.33	0.829
Eu^{3+}	3.0×10^{-3}	0.0010	0.403	4.51	0.935
	2.5×10^{-2}	0.0080	0.457	4.40	0.883
	5.0×10^{-2}	0.015	0.475	4.36	0.865

[a] Determined from the equation ΔG_{ET} $(M^{n+}) = 1.19 - 0.059 \log(K_{red}[M^{n+}])$. [b] Determined from eq 8.

The ESR spectra were measured upon addition of $Y(OTf)_3$ or $Sc(OTf)_3$ (2.0×10^{-2} M) to an MeCN solution of **Fc-NQ** (9.1×10^{-3} M) to confirm the formation of $\mathbf{Fc^+}$-$\mathbf{NQ^{\bullet-}/Y^{3+}}$ and $\mathbf{Fc^+}$-$\mathbf{NQ^{\bullet-}/Sc^{3+}}$ complexes at 298 K. The observed ESR spectra are shown in Figure 3a ($\mathbf{Fc^+}$-$\mathbf{NQ^{\bullet-}/Y^{3+}}$) and Figure 3b ($\mathbf{Fc^+}$-$\mathbf{NQ^{\bullet-}/Sc^{3+}}$). The *g* values are determined as 2.0037 ($\mathbf{Fc^+}$-$\mathbf{NQ^{\bullet-}/Y^{3+}}$) and 2.0038 ($\mathbf{Fc^+}$-$\mathbf{NQ^{\bullet-}/Sc^{3+}}$). The hyperfine structures are quite different depending on the type of metal ion. This indicates the binding of metal ions with the $NQ^{\bullet-}$ moiety of $\mathbf{Fc^+}$-$\mathbf{NQ^{\bullet-}}$. The hyperfine coupling (hfc) constants are determined by the computer simulation spectra (see Supporting Information S1). In contrast to the instability of the metal ion complexes of radical anions of *p*-benzoquinone derivatives,[26a] the $\mathbf{Fc^+}$-$\mathbf{NQ^{\bullet-}/M^{n+}}$ complex particularly in the case of the Sc^{3+} complex is very stable even at 298 K.[36] Such a remarkable stability of the $\mathbf{Fc^+}$-$\mathbf{NQ^{\bullet-}/M^{n+}}$ complex may be ascribed to the hydrogen bonding of the amide proton with one carbonyl oxygen of the semi-

(33) (a) Baerends, E. J.; Ellis, D. E.; Ros, P. *Chem. Phys.* **1973**, *2*, 41. (b) te Valde, B.; Baerends, E. J. *J. Comput. Phys.* **1992**, *99*, 84.
(34) The absorption band at 860 nm due to Fc^+ in **Fc-NQ** was confirmed by electron-transfer oxidation by **Fc-NQ** with $Ru(bpy)_3(PF_6)_3$.
(35) Fukuzumi, S.; Ohkubo, K. *J. Am. Chem. Soc.* **2002**, *124*, 10270.

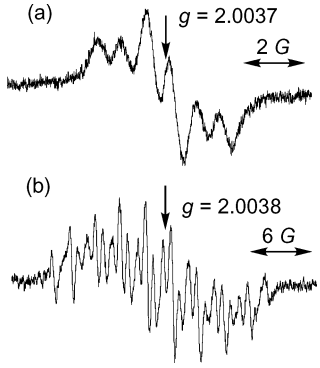

Figure 3. (a) ESR spectrum of **Fc-NQ** (9.1×10^{-3} M) in the presence of Y^{3+} (2.0×10^{-2} M) in deaerated MeCN at 298 K. (b) ESR spectrum of **Fc-NQ** (9.1×10^{-3} M) in the presence of Sc^{3+} (2.0×10^{-2} M) in deaerated MeCN at 298 K.

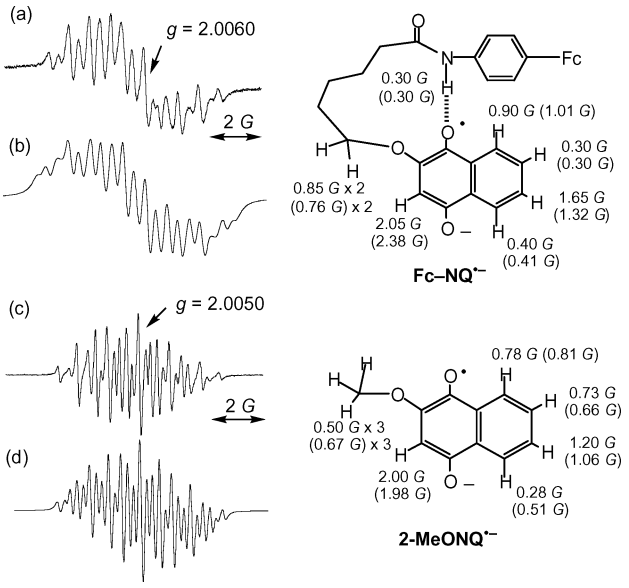

Figure 4. (a) ESR spectrum of **Fc-NQ**•– (4.0×10^{-3} M) in deaerated MeCN at 298 K and (b) the computer simulation spectrum (the values in parentheses are provided by ADF calculation). (c) ESR spectrum of 2-MeONQ•– (5.0×10^{-5} M) in deaerated MeCN at 298 K and (d) the computer simulation spectrum (the values in parentheses are provided by ADF calculation).

quinone radical anion. The presence of the hydrogen bond in the radical anion of **Fc-NQ** was confirmed by examining the spin density distribution of **Fc-NQ**•– and the radical anion of 2-methoxy-1,4-naphthoquinone (2-MeONQ•–) as follows.

Fc-NQ•– is produced by the electron-transfer reduction of **Fc-NQ** by naphthalene radical anion (Scheme 3). The ESR spectrum of **Fc-NQ**•– thus produced is shown in Figure 4a together with the computer simulation spectrum (Figure 4b). The *g* value of **Fc-NQ**•– in Figure 4a is determined as 2.0060, which is significantly larger than those of the metal ion complexes in Figure 3. This indicates that more spin is localized on the oxygen atom which has a large spin−orbit coupling constant in the case of **Fc-NQ**•– as compared to those of the metal ion complexes. The simulated hyperfine coupling constants (hfc) can be well reproduced by the ADF calculation of

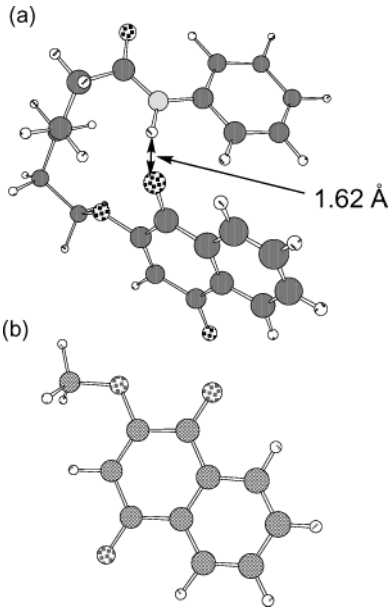

Figure 5. Optimized structures of (a) **Ph-NQ**•– and (b) 2-MeONQ•– obtained by ADF calculation with the II (large) basis set.

Ph-NQ•– in which the Fc moiety is omitted as indicated in Figure 4 (the values in parentheses).[37] The optimized structures of **Ph-NQ**•– and 2-MeONQ•– obtained by the Amsterdam density function (ADF) calculation with the II (large) basis set are shown in Figure 5. The O−H distance between the carbonyl oxygen of NQ•– and the amide proton in **Ph-NQ**•– is 1.62 Å. This value is even shorter than the hydrogen bonding distance between the semiquinone radical anion and water (1.78 Å).[38]

The radical anion (2-MeONQ•–) without hydrogen bonding is also produced by the electron-transfer reduction of 2-MeONQ by the naphthalene radical anion as shown in Figure 4c. The simulated hfc values can also be well reproduced by the ADF calculation as indicated in Figure 4d (the values in parentheses), and they are quite different from those observed in **Fc-NQ**•– with hydrogen bonding.

Change in the One-Electron Reduction Potential of Fc-NQ in the Presence of Metal Ions. The remarkable stability of **Fc**$^+$**-NQ**•–**/M**$^{n+}$ complexes mentioned above allows us to determine the one-electron reduction potentials of **Fc-NQ** (E_{red}) in the presence of various concentrations of metal ions by cyclic voltammetry measurements as shown in Figure 6. The one-electron reduction potential of the NQ moiety is observed as a well-defined reversible wave at −0.81 V (Figure 6a).[39] In the presence of 7.0×10^{-3} M Sc^{3+}, the E_{red} value exhibits a remarkable positive shift from −0.81 to 1.26 V,[40] whereas the one-electron oxidation potential of the Fc moiety remains the same irrespective of the absence or presence of Sc^{3+} (Figure 6b). The cyclic voltammograms of **Fc-NQ** in the presence of various concentrations of Sc^{3+} are shown in the Supporting

(36) The semiquinone radical anion complexes with metal ions have been only observed only at low temperature by ESR.[26a] In contrast, the **Fc**$^+$**−NQ**•–**/Sc**$^{3+}$ complex has a long lifetime (>3 h) at 298 K. The **Fc**$^+$**−Q**•–**/Sc**$^{3+}$ complex reported in ref 21 is also too unstable to detect the ESR spectrum at 298 K because of the fast disproportionation of the Q•–/Sc^{3+} complex.

(37) The hfc values were also calculated using the B3LYP method. The ADF calculation predicts the hfc values in closer agreement with the experimental results.

(38) O'Malley, P. J. *Phys. Chem. A* **1997**, *101*, 6334.

(39) The one-electron oxidation potential for the Fc^+/Fc couple in **Fc-NQ** agrees with that of ferrocene (E_{ox}^0 vs SCE = 0.37 V), see: Fukuzumi, S.; Mochizuki, S.; Tanaka, T. *Inorg. Chem.* **1989**, *28*, 2459.

(40) The anodic peak current for the oxidation of the **Fc-NQ**•–**/Sc**$^{3+}$ complex is smaller than the cathodic peak current for the reduction of **Fc-NQ** in the presence of Sc^{3+} because of the instability of the **Fc-NQ**•–**/Sc**$^{3+}$ complex. A similar trend is observed for cyclic voltammograms of **Fc-NQ** in the presence of other metal ions.

Scheme 3

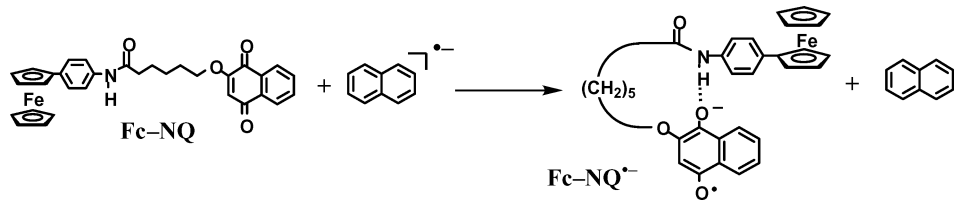

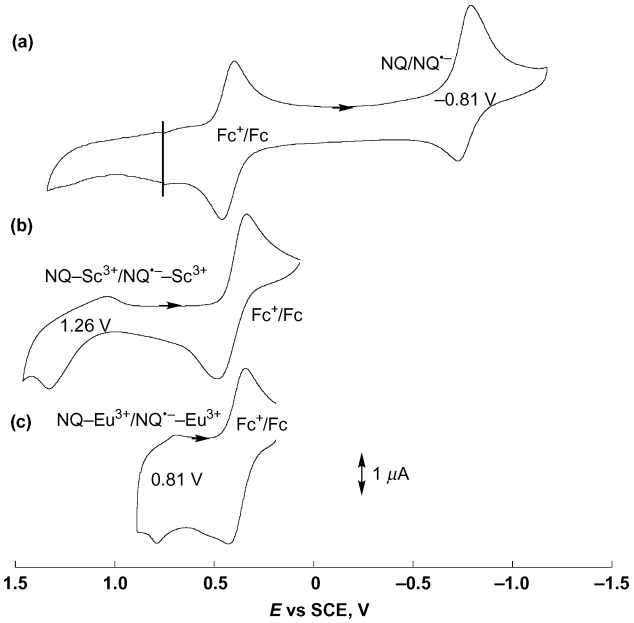

Figure 6. (a) Cyclic voltammogram of **Fc-NQ** (5.0×10^{-4} M) in deaerated MeCN containing 0.1 M Bu_4NPF_6 at 298 K with sweep rate of 50 mV s^{-1}. (b) Cyclic voltammogram of **Fc-NQ** (5.0×10^{-4} M) in the presence of Sc^{3+} (7.0×10^{-3} M) in deaerated MeCN containing 0.1 M Bu_4NPF_6 at 298 K with sweep rate of 50 mV s^{-1}. (c) Cyclic voltammogram of **Fc-NQ** (5.0×10^{-4} M) in the presence of Eu^{3+} (7.0×10^{-3} M) in deaerated MeCN containing 0.1 M Bu_4NPF_6 at 298 K with sweep rate of 100 mV s^{-1}.

Information (S2). Similar positive shifts of E_{red} are observed in the presence of Eu^{3+} (Figure 6c) and Y^{3+} (S3).

The positive shift of E_{red} in the presence of metal ion is ascribed to the binding of metal ion with $NQ^{\bullet-}$ (eq 4) as indicated in Figure 3. In such a case, E_{red} is given as a function

$$\text{Fc-NQ}^{\bullet-} + \text{M}^{n+} \overset{K_{red}}{\rightleftharpoons} \text{Fc-NQ}^{\bullet-}/\text{M}^{n+} \qquad (4)$$

of the concentration of M^{n+}, in accordance with the Nernst equation (eq 5), where E_{red}^0 is the one-electron reduction potential in the absence of metal ion, K_{red} is the formation constant of the **Fc-NQ**$^{\bullet-}$/$\mathbf{M}^{n+}$ complex, and K_{ox} is the formation constant of the **Fc-NQ**/$\mathbf{M}^{n+}$ complex.[41]

$$E_{red} = E_{red}^0 + (2.3RT/F) \times \log\{(1 + K_{red}[\text{M}^{n+}])/(1 + K_{ox}[\text{M}^{n+}])\} \qquad (5)$$

Because $K_{red}[M^{n+}] \gg 1$, and $K_{ox}[M^{n+}] \ll 1$, eq 5 is written by eq 6, where ΔE_{red} is the potential shift in the presence of M^{n+}

$$\Delta E_{red} = (2.3RT/F) \log K_{red}[\text{M}^{n+}] \qquad (6)$$

from the value in its absence.

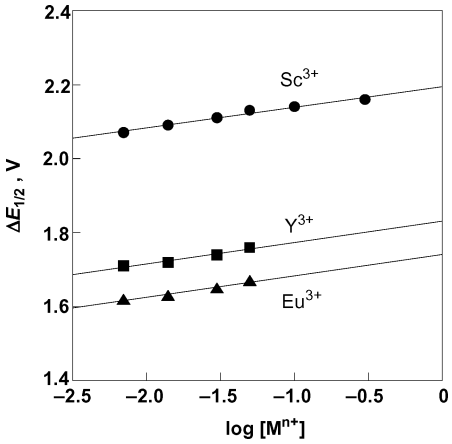

Figure 7. Plots of $\Delta E_{1/2}$ versus log[M^{n+}] for the one-electron reduction of **Fc-NQ** in the presence of Sc^{3+} (●), Y^{3+} (■), and Eu^{3+} (▲) in MeCN at 198 K. The plot of each [M^{n+}] affords the same slope of 0.059.

The plots of ΔE_{red} versus log[M^{n+}] ($M^{n+} = Sc^{3+}$, Y^{3+}, and Eu^{3+}) are shown in Figure 7.

The slope of each plot is determined as 0.059, which agrees with the expected slope (=2.3*RT*/*F* at 298 K) by the Nernst equation (eq 6). The intercepts of linear plots in Figure 7 thus afford the binding constants $K_{red}(Sc^{3+}) = 1.6 \times 10^{37}$ M^{-1}, $K_{red}(Y^{3+}) = 1.1 \times 10^{31}$ M^{-1}, and $K_{red}(Eu^{3+}) = 3.3 \times 10^{29}$ M^{-1}. The K_{red} values correspond to the free energy changes of the metal ion binding: 2.20 eV (Sc^{3+}), 1.83 eV (Y^{3+}), and 1.74 eV (Eu^{3+}).[42] Such a large binding energy results in a remarkable change in the driving force of electron transfer in **Fc-NQ** from a highly negative value to a positive value in the presence of M^{n+}. The driving force of electron transfer in the presence of M^{n+} ($-\Delta G_{ET}$) is given by eq 7

$$-\Delta G_{ET} = -\Delta G_{ET}^0 + RT \ln(K_{red}[\text{M}^{n+}]) \qquad (7)$$

where $-\Delta G_{ET}^0$ is the driving force in the absence of M^{n+}. The $-\Delta G_{ET}$ values determined in the presence of various concentrations of M^{n+} are summarized in Table 1.

Driving Force Dependence of Metal Ion-Promoted Electron Transfer. Figure 8 shows the driving force dependence of log k_{ET} of M^{n+}-promoted electron transfer, where the k_{ET} and $-\Delta G_{ET}^0$ values are taken from Table 1. Three separate linear correlations are obtained for the case of Sc^{3+}, Y^{3+}, and Eu^{3+} (Figure 8). The slope of each linear plot is determined as 16.9 $(eV)^{-1}$, which corresponds to $1/2.3k_BT$ at 298 K, where k_B is the Boltzmann constant. This indicates that the change in driving force with concentration of M^{n+} is directly reflected on the change in the activation free energy, that is, $\partial(\Delta G_{ET}^{\ddagger})/\partial(\Delta G_{ET}) = 1$. This is quite different from the slope expected from the Marcus equation (eq 1): $\partial(\Delta G_{ET}^{\ddagger})/\partial(\Delta G_{ET})$

(41) Meites, L. *Polarographic Techniques*, 2nd ed.; Wiley: New York, 1965; pp 203−301.

(42) Binding free energy changes are calculated as the follow equation: (binding free energy changes) = $-RT \ln K_{red}$.

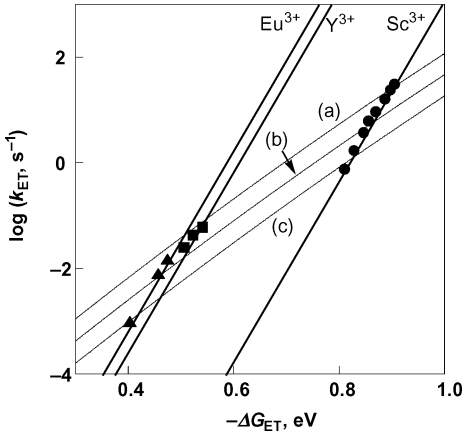

Figure 8. Plots of log k_{ET} versus $-\Delta G_{ET}$ in M^{n+}-promoted intramolecular electron transfer in **Fc-NQ** in the addition of Sc^{3+} (●), Y^{3+} (■), and Eu^{3+} (▲) in deaerated MeCN at 298 K. The plot of k_{ET} on each $[M^{n+}]$ gives a straight line with a slope of 16.9. The broken lines (a), (b), and (c) represent the fit to eq 9 with (a) $\lambda = 4.3$ eV, (b) $\lambda = 4.4$ eV, and (c) $\lambda = 4.5$ eV.

Scheme 4

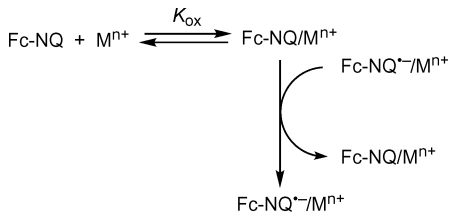

$= 0.5$. The driving force dependence of k_{ET} expected from the Marcus equation is shown as broken lines in Figure 8, where three different λ_{DA} values (4.3, 4.4, and 4.5 eV) are used for the calculation using eq 1. The $\Delta G^{\ddagger}_{ET}$ value is converted to the corresponding k_{ET} value using eq 8, by assuming that the M^{n+}-

$$k_{ET} = (k_B T/h) \exp(-\Delta G^{\ddagger}_{ET}/k_B T) \quad (8)$$

promoted intramolecular electron transfer in **Fc-NQ** is adiabatic.[43] Hereby, h is the Planck constant. From the comparison of the calculated Marcus lines with the observed lines, it is apparent that the λ_{DA} value changes with the concentration of M^{n+}. Such a change of λ_{DA} with $[M^{n+}]$ can be evaluated within the context of the Marcus theory of electron transfer (vide infra).

The λ_{DA} value consists of λ_D for the electron self-exchange between D and $D^{\bullet+}$ and λ_A for that between A and $A^{\bullet-}$ (eq 3). Because the metal ion is involved only in the acceptor part, the dependence of λ_A on $[M^{n+}]$ should be considered. The electron self-exchange between **Fc-NQ** and the **Fc-NQ**$^{\bullet-}$/**M**$^{n+}$ complex occurs via formation of the **Fc-NQ/M**$^{n+}$ complex as shown in Scheme 4. According to Scheme 4, the electron self-exchange rate constant (k_{ex}) is given by eq 9, where Z is the frequency factor for an intermolecular reaction, and $\lambda_A{}^0$ is the reorganiza-

$$k_{ex} = ZK_{ox}[M^{n+}] \exp(-\lambda_A{}^0/4k_B T) \quad (9)$$

tion energy for the electron self-exchange between **Fc-NQ/M**$^{n+}$ and **Fc-NQ**$^{\bullet-}$/**M**$^{n+}$. The reorganization energy between **Fc-NQ** and **Fc-NQ**$^{\bullet-}$/**M**$^{n+}$ (λ_A) is then given by eq 10, by comparing eq 9 with $k_{ex} = Z \exp(-\lambda_A/4k_B T)$. From eq 3, the reorganization

(43) Because **Fc-NQ** has a long flexible methylene spacer, there may be sufficient interaction between the Fc and NQ moieties to make the electron transfer adiabatic.

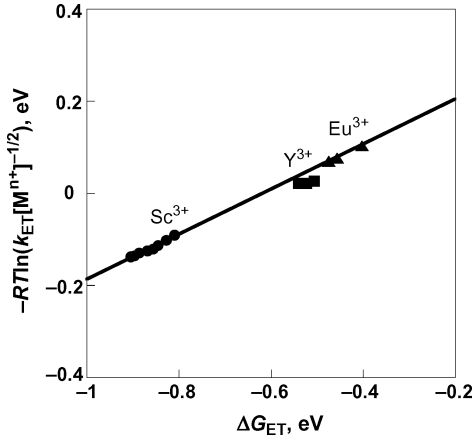

Figure 9. Plots of $-RT \ln(k_{ET}[M^{n+}]^{-1/2})$ versus ΔG_{ET} in M^{n+}-promoted intramolecular electron transfer in **Fc-NQ** in the addition of Sc^{3+} (●), Y^{3+} (■), and Eu^{3+} (▲) in deaerated MeCN at 298 K. The plot of $-RT \ln(k_{ET}[M^{n+}]^{-1/2})$ versus ΔG_{ET} on each $[M^{n+}]$ gives a straight line with a slope of 0.5.

energy λ_{DA} is given by eq 11, where $\lambda_{DA}{}^0 = (\lambda_D + \lambda_A{}^0)/2$. Equation 11 indicates that the λ_{DA} value decreases with increasing $[M^{n+}]$ as observed in Figure 8.

$$\lambda_A = \lambda_A{}^0 - 4RT \ln(K_{ox}[M^{n+}]) \quad (10)$$

$$\lambda_{DA} = \lambda_{DA}{}^0 - 2RT \ln(K_{ox}[M^{n+}]) \quad (11)$$

Because $\lambda_{DA} \gg -\Delta G_{ET}$ in Figure 8, eq 1 is simplified to eq 12 under the present experimental conditions. The driving force dependence of k_{ET} is derived from eqs 8, 11, and 12 as eq 13

$$\Delta G^{\ddagger}_{ET} = (\lambda_{DA}/4) + (\Delta G_{ET}/2) \quad (12)$$

$$-RT \ln(k_{ET}/[M^{n+}]^{1/2}) = C + (\Delta G_{ET}/2) \quad (13)$$

where C is a constant which is independent of the concentration of M^{n+}, given by eq 14.

$$C = (\lambda_{DA}{}^0/4) - RT \ln[k_B T(K_{ox})^{1/2}/h] \quad (14)$$

A plot of $-RT \ln(k_{ET}/[M^{n+}]^{1/2})$ versus ΔG_{ET} including all of the data in Table 1 is shown in Figure 9, where a single linear correlation is obtained. The slope is determined as 0.5, which agrees with expectation from eq 13.

The single linear correlation in Figure 9 indicates that the C value is constant irrespective of the type of metal ions. The larger the binding between $NQ^{\bullet-}$ and M^{n+}, the larger is the $\lambda_{DA}{}^0$ value and also the larger is the K_{ox} value for the binding between NQ and M^{n+}. In such a case, the effects of different metal ions may be largely canceled in the C value in eq 14.

The large reorganization energy involved in the M^{n+}-promoted electron transfer was also confirmed by the temperature dependence of k_{ET}. Eyring plots of Sc^{3+}-promoted electron transfer in **Fc-NQ** are shown in Figure 10. The activation parameters obtained from the Eyring plots are listed in Table 2. The same activation enthalpy ($\Delta H^{\ddagger}_{obs} = 52$ kJ mol^{-1} $= 0.54$ eV) is obtained irrespective of the difference in Sc^{3+} concentration (Table 2). The observed activation enthalpy ($\Delta H^{\ddagger}_{obs}$) consists of the activation enthalpies of the electron self-exchange between the donor Fc and Fc^{+} ($\Delta H^{\ddagger}_{D}$) and between the acceptor NQ and $NQ^{\bullet-}$ ($\Delta H^{\ddagger}_{A}$): $\Delta H^{\ddagger}_{obs} = (\Delta H^{\ddagger}_{D} + \Delta H^{\ddagger}_{A})/2$.

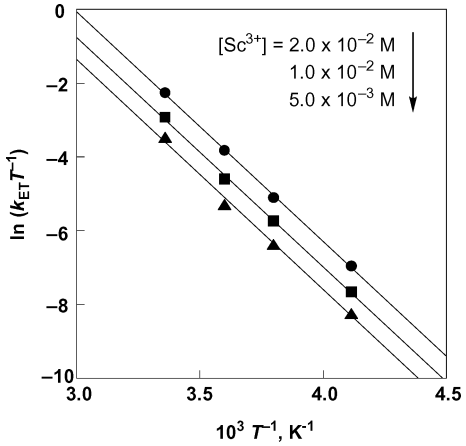

Figure 10. Eyring plots of $\ln(k_{ET}T^{-1})$ versus T^{-1} in M^{n+}-promoted intramolecular electron transfer in **Fc-NQ** (2.0×10^{-4} M) in the presence of Sc^{3+} [2.0×10^{-2} M (●), 1.0×10^{-2} M (■), and 5.0×10^{-3} M (▲)] in deaerated MeCN.

Table 2. Activation Parameters for Sc^{3+}-Promoted Intramolecular Electron Transfer in **Fc-NQ** with Various Concentrations of $Sc(OTf)_3$ in Deaerated MeCN at 298 K

$[Sc^{3+}]$, M	$\Delta H^{\ddagger}_{obs}$, kJ mol^{-1}	$\Delta S^{\ddagger}_{obs}$, J K^{-1}mol^{-1}	$\Delta G^{\ddagger}_{obs}$, eV[a]
5.0×10^{-3}	52	−53	0.701
1.0×10^{-2}	52	−49	0.686
2.0×10^{-2}	52	−43	0.667

[a] $T = 298$ K.

Using this relation, we determined the $\Delta H^{\ddagger}_A$ value as 0.86 eV from the $\Delta H^{\ddagger}_{obs}$ value (0.54 eV) and the reported value of $\Delta H^{\ddagger}_D$ (0.22 eV).[44] Thus, the $\lambda_A{}^0$ value for the electron self-exchange between NQ/Sc^{3+} and $NQ^{\bullet-}/Sc^{3+}$ is estimated as $\lambda_A{}^0 > 3.44$ eV, because $\lambda_A{}^0 = 4(\Delta H^{\ddagger}_A - T\Delta S^{\ddagger})$ and $\Delta S^{\ddagger}_A < 0$. The reorganization energy $\lambda_A{}^0$ consists of twice the stabilization energy of the $NQ^{\bullet-}/Sc^{3+}$ complex with the optimized structure as compared to the $NQ^{\bullet-}/Sc^{3+}$ complex with the same nuclear configuration as the neutral NQ/Sc^{3+} complex.[45] Because the stabilization free energy is obtained as 2.20 eV, which is derived from the K_{red} value for the $NQ^{\bullet-}/Sc^{3+}$ complex (vide supra), the $\lambda_A{}^0$ value is estimated as 4.40 eV. This value is consistent with the estimation from the $\Delta H^{\ddagger}_A$ value: $\lambda_A{}^0 > 3.44$ eV.

In conclusion, metal ion-promoted intramolecular electron transfer in **Fc-NQ** proceeds via strong binding of the $NQ^{\bullet-}$ moiety with metal ion, which results in a drastic change of the free energy change of electron transfer from a highly positive value to a highly negative value. Such a drastic change of driving force of electron transfer is accompanied by a large reorganization energy required for the metal ion-promoted electron transfer. The driving force dependence of k_{ET} of the metal ion-promoted intramolecular electron transfer can be well evaluated within the context of the Marcus theory of electron transfer in which the driving force increases with increasing concentrations of metal ions, whereas the reorganization energy of electron transfer decreases with concentrations of metal ions.

Acknowledgment. This work was supported by the Academy of Finland, the National Technology Agency of Finland, and Grant-in-Aids (No. 11740352 to H.I., Nos. 11555230 and 11694079 to S.F.) and the Development of Innovative Technology (No. 12310) from the Ministry of Education, Science, Sports, and Culture, Japan. H.I. thanks the Nagase Foundation for financial support.

Supporting Information Available: ESR simulation of $\mathbf{Fc^{+}}$-$\mathbf{NQ^{\bullet-}/M^{n+}}$ (S1), CVs of **Fc-NQ** in the presence of Sc^{3+} (S2), and CV and SHACV of **Fc-NQ** in the presence of Y^{3+} (S3) (PDF). This material is available free of charge via the Internet at http://pubs.acs.org.

JA034831R

(44) (a) Yang, E. S.; Chan, M.-S.; Wahl, A. C. *J. Phys. Chem.* **1980**, *84*, 3094. (b) Fukuzumi, S.; Nakanishi, I.; Suenobu, T.; Kadish, K. M. *J. Am. Chem. Soc.* **1999**, *121*, 3468.

(45) The stabilization energy of the $NQ^{\bullet-}/Sc^{3+}$ complex is equal to the destabilization of the NQ/Sc^{3+} complex with the same nuclear configuration as the $NQ^{\bullet-}/Sc^{3+}$ complex as compared to the NQ/Sc^{3+} complex with the optimized structure.